Applied Energy 255 (2019) 113856

Contents lists available at ScienceDirect

Applied Energy

journal homepage: www.elsevier.com/locate/apenergy

Output characteristics of thin-film flexible piezoelectric generators: A numerical and experimental investigation

Jie Chen[a,b,c,d], Noor Nabulsi[a], Weijie Wang[a,c,d], Ja Yeon Kim[e], Min-Ki Kwon[f], Jae-Hyun Ryou[a,b,c,d,*]

[a] Department of Mechanical Engineering, University of Houston, Houston, TX 77204-4006, USA
[b] Materials Science and Engineering Program, University of Houston, Houston, TX 77204, USA
[c] Advanced Manufacturing Institute (AMI), University of Houston, Houston, TX 77204, USA
[d] Texas Center for Superconductivity at UH (TcSUH), University of Houston, Houston, TX 77204, USA
[e] Korea Photonics Technology Institute (KOPTI), Gwangju 61007, Republic of Korea
[f] Department of Photonic Engineering, Chosun University, Gwangju 61452, Republic of Korea

HIGHLIGHTS

- Piezoelectric generator design based on polarization.
- Flexible piezoelectric generator simulation with a buckle-bending model.
- Piezoelectric output characteristics investigation by simulation and experiment.
- Device optimization based on piezoelectric output behavior.

GRAPHICAL ABSTRACT

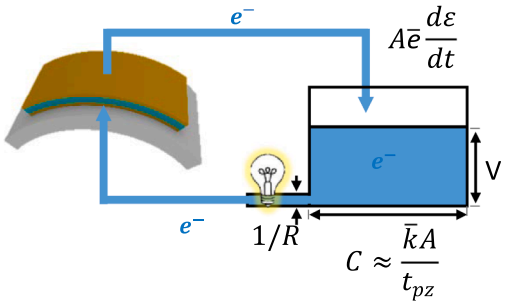

ARTICLE INFO

Keywords:
Flexible
Piezoelectric
Nanogenerators
Output characteristics

ABSTRACT

Flexible piezoelectric generators are promising energy harvesters for future self-powered electronics by converting surrounding mechanical energy into electricity. Although many types of flexible piezoelectric generators have been demonstrated, their output behaviors are still not systematically reported due to the complexity since the behaviors depend on many ingredients including piezoelectric device parameters and external mechanical energy conditions. In this research, numerical simulations based on a buckle-bending model were carried out to systematically investigate the output characteristics of flexible piezoelectric generators. The reliability of the numerical results were verified through experimentation using group III-nitride thin-film flexible piezoelectric generators. The ideal open-circuit voltage and short-circuit current density are proportional to the strain and strain rate of the piezoelectric material, respectively. For a specific device at a certain mechanical condition, the piezoelectric output varies with load resistance and shows a maximum power density at a certain load resistance, i.e., optimum load resistance. The optimum load resistance increases linearly with piezoelectric material thickness, inverse of device area, and bending time, while does not change with flexible substrate thickness, and bending extent. The optimum power density increases linearly with piezoelectric material thickness, square of flexible substrate thickness, inverse of bending time, and bending extent, while does not change with device area. The detailed understanding of the output characteristics of flexible piezoelectric generators can help the optimization of device configuration for better piezoelectric energy harvesting.

* Corresponding author.
E-mail address: jryou@uh.edu (J.-H. Ryou).

https://doi.org/10.1016/j.apenergy.2019.113856
Received 5 June 2019; Received in revised form 27 July 2019; Accepted 3 September 2019

1. Introduction

With increasing applications of health and environmental monitoring electronics [1,2], traditional power supply options face technological advancement demands, since both small size and long service time are preferred. Disposable or rechargeable batteries, the most widely used power supplies, fall short of these demands due to constant battery replacement or recharging, which is impossible in large amounts. Therefore, the concept of self-powered electronics have been proposed to solve this problem since an endless amount of electricity can be scavenged from the surroundings by energy harvesters [3,4]. Among the energy harvesters, piezoelectric generators and triboelectric generators are starting to attract a lot of attention since they can convert the widely available mechanical energy into electricity [5–8]. This capability is especially suitable for wearable or implantable applications since a large amount of biomechanical energy is readily available [9,10]. The generators are preferred to be flexible in order to have a better interface with the soft human body. A wide variety of flexible piezoelectric generators have been developed recently, such as flexible piezoelectric generators (F-PEGs) using lead zirconate titanate (PZT, Pb$[Zr_xTi_{1-x}]O_3$) [11,12], polyvinylidene difluoride (PVDF) [13,14], barium titanate ($BaTiO_3$) [15,16], zinc stannate ($ZnSnO_3$) [17,18], zinc oxide (ZnO) [19,20], group III-nitride (III-N) thin films [21–23], and composite thin films [24]. Although increased piezoelectric output power has been demonstrated by these F-PEGs, few researchers have systematically studied the output behavior due to its complicated dependence on both the piezoelectric device parameters and external mechanical energy conditions. In practical applications, especially for system level design, the output requirement for F-PEGs such as the optimum load resistance, voltage, current, and power level may vary from case to case. It is unrealistic to make a large number of generators by trial and error to design a suitable F-PEG for each application. Therefore, theoretical studies based on a reliable model is required to help investigate the piezoelectric output comprehensively [25,26]. However, traditional theories developed for piezoelectric generators working by vibration mode [27–29] cannot be applied directly since F-PEGs usually work at low frequencies with non-vibration mode, for example devices attached onto skin surface to harvest biomechanical energy. A buckle-bending model has been proposed recently to simulate a PZT ribbon based F-PEG [30], showing a voltage and current response complying well with the experimental results, indicating its feasibility to simulate the piezoelectric output of F-PEGs.

In the present study, output characteristics of flexible piezoelectric generators were systematically studied by both numerical simulation with the buckle-bending model and experimental tests using the III-N thin-film F-PEG as an example. The results from the numerical simulation and experiment were compared in order to confirm the validity of the model. The investigated relationships include: piezoelectric thin-film strain and open-circuit voltage, strain rate and short-circuit current, and power change with load resistance. Additionally, the effect of external mechanical conditions, such as degree of bending and bending speed, as well as the effect of device parameters such as device area and flexible substrate thickness on optimum load resistance, voltage, current density, and power density were investigated systemically. The results can also be useful to design other types of flexible piezoelectric generators.

2. Numerical and experimental methods

2.1. Device structure and operating conditions

Many kinds of piezoelectric thin films have a polarization direction perpendicular to the thin film surface, i.e., along the surface normal, as schematically shown in Fig. 1a. Examples include: the wurtzite structure thin films grown on basal-plane (Supplementary Material Fig. A.1), such as GaN, AlN, and ZnO, and ferroelectric thin films that are polarized by a vertical electric field. When a uniaxial compressive or uniaxial tensile strain is applied on such thin films, for example by bending, the change of polarization occurs along the surface normal direction, as shown in Fig. 1b–c. Since piezoelectricity is caused by a change in polarization [31], the piezoelectric thin film shows a potential difference only along the vertical direction, which was confirmed by the COMSOL simulation results shown in Fig. 1d. As a result, piezoelectric devices with polarization along the surface normal generally require a sandwich structure with top and bottom electrodes [22,32], as schematically shown in Fig. 1e.

The piezoelectric thin film can be assumed at plane-strain condition during bending with top surface traction free [30], since its thickness,

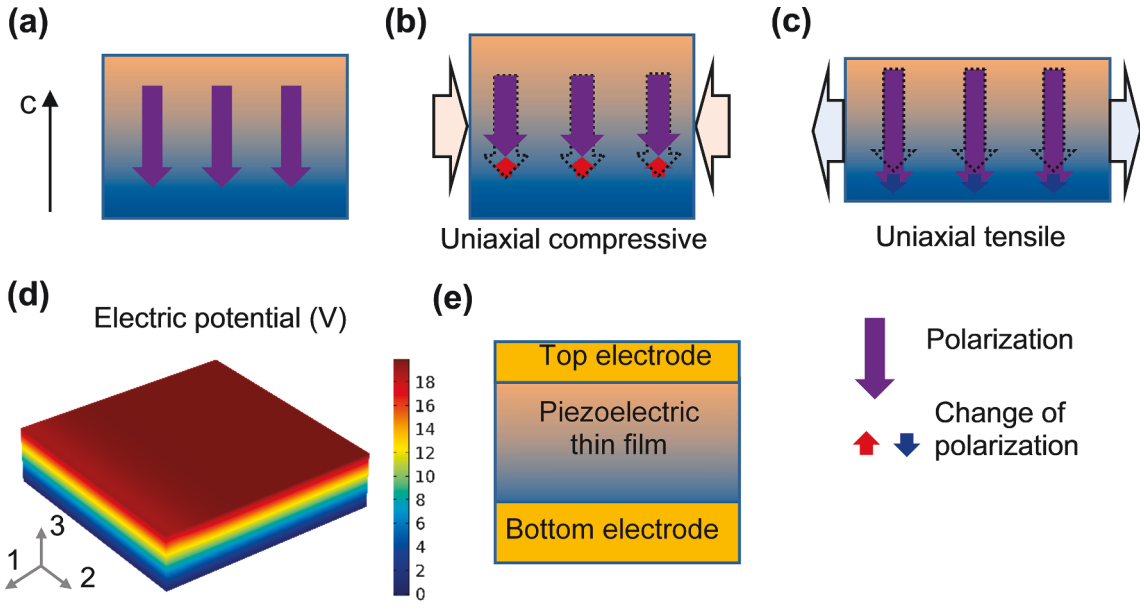

Fig. 1. Piezoelectric device design based on polarization. Schematic illustration of piezoelectric thin film with polarization perpendicular to the thin film, (a) without strain, (b) with uniaxial compressive strain, and (c) with uniaxial tensile strain. (d) Potential distribution on the piezoelectric thin film when uniaxial strain is applied, obtained by COMSOL simulation. (e) Schematic illustration of the sandwich device structure, with top and bottom electrodes on the top and bottom surfaces of the piezoelectric thin film, respectively.

several nanometers to micrometers, is much smaller than its lateral dimension, several millimeters to centimeters, resulting the strain in bending axis direction negligible. Under the plane-strain approximation, both the piezoelectric coefficient and dielectric permittivity can be simplified and related to the thin film uniaxial strain. The effective piezoelectric coefficient $\bar{e}$ can be reduced to [30],

$$\bar{e} = e_{31} - \frac{c_{13}}{c_{33}} e_{33} \tag{1}$$

where e_{31} and e_{33} are piezoelectric coefficients, c_{13} and c_{33} are elastic constants. The III-N thin film is transversely isotropic with polarization direction 3 (i.e., c-axis) normal to the surface. For III-N thin films, $\bar{e} < 0$. The effective dielectric permittivity $\bar{k}$ can be reduced to [30],

$$\bar{k} = k_{33} + \frac{e_{33}^2}{c_{33}} \tag{2}$$

where k_{33} is the dielectric permittivity along thin film normal direction.

2.2. Output of flexible piezoelectric generator

Since piezoelectricity originates from Maxwell's displacement current [33], the piezoelectric generator can be modeled by an equivalent circuit as shown in Fig. 2a, a current source coupled with a capacitor and a resistor [34]. The current source is the electric displacement current I_D, as a result of mechanical energy applied on the piezoelectric thin film,

$$I_D = A\frac{d}{dt}D = A\frac{d}{dt}P = A\frac{d}{dt}(\bar{e}\varepsilon) = A\bar{e}\frac{d\varepsilon}{dt} \tag{3}$$

where D is the electric displacement, or surface charge density of the dielectric, P is the polarization, which is equal to D when no external electric field is applied, ε is the uniaxial strain of the piezoelectric thin film while bent, and A is the effective device area, i.e., the overlap area between the top and bottom electrodes. The capacitance C of the capacitor can be calculated as,

$$C = \frac{\bar{k}A}{t_{pz}(1-\nu\varepsilon)} \approx \frac{\bar{k}A}{t_{pz}} \tag{4}$$

where ν and t_{pz} is Poisson's ratio and the thickness of the piezoelectric thin film, respectively. For a good piezoelectric device, the parasitic resistor can be neglected since its resistance R_P should be very high ($> G\Omega$).

When measuring the short-circuit current, as shown in Fig. 2d, both the capacitor and parasitic resistor are shorted by the electrometer. The measured short-circuit current I_{sc} equals to the displacement current I_D,

$$I_{sc} = I_D = A\bar{e}\frac{d\varepsilon}{dt} \tag{5}$$

When measuring the open-circuit voltage, as shown in Fig. 2e, the voltage will be determined by the electric charge Q collected on the capacitor. If neglecting the parasitic resistance, the ideal open-circuit voltage V_{oc} can be calculated as,

$$V_{oc} = \frac{Q}{C} = \frac{AD}{C} = \frac{A(\bar{e}\varepsilon)}{\frac{\bar{k}A}{t_{pz}}} = \frac{\bar{e}}{\bar{k}} t_{pz}\varepsilon \tag{6}$$

The electrical energy W_e stored in the piezoelectric material under applied strain is,

$$W_e = \frac{1}{2}CV_{oc}^2 = \frac{1}{2}(At_{pz})\frac{\bar{e}^2}{\bar{k}}\varepsilon^2 \tag{7}$$

In addition to the piezoelectric coefficients and dielectric permittivities, which are determined by the quality and type of piezoelectric materials, the generated piezoelectricity is also related to the device parameters such as device area, piezoelectric thin film thickness, and the applied uniaxial strain on the piezoelectric thin film. For certain piezoelectric materials under a fixed strain condition, the generated piezoelectricity is proportional to the volume of piezoelectric material in the device. As a result, piezoelectric generators using nanoparticles [32], nanowires [35], or porous structures dispersed in polymer matrix [36] may improve in flexibility and durability; however, their piezoelectric output will be compromised due to a less effective piezoelectric volume.

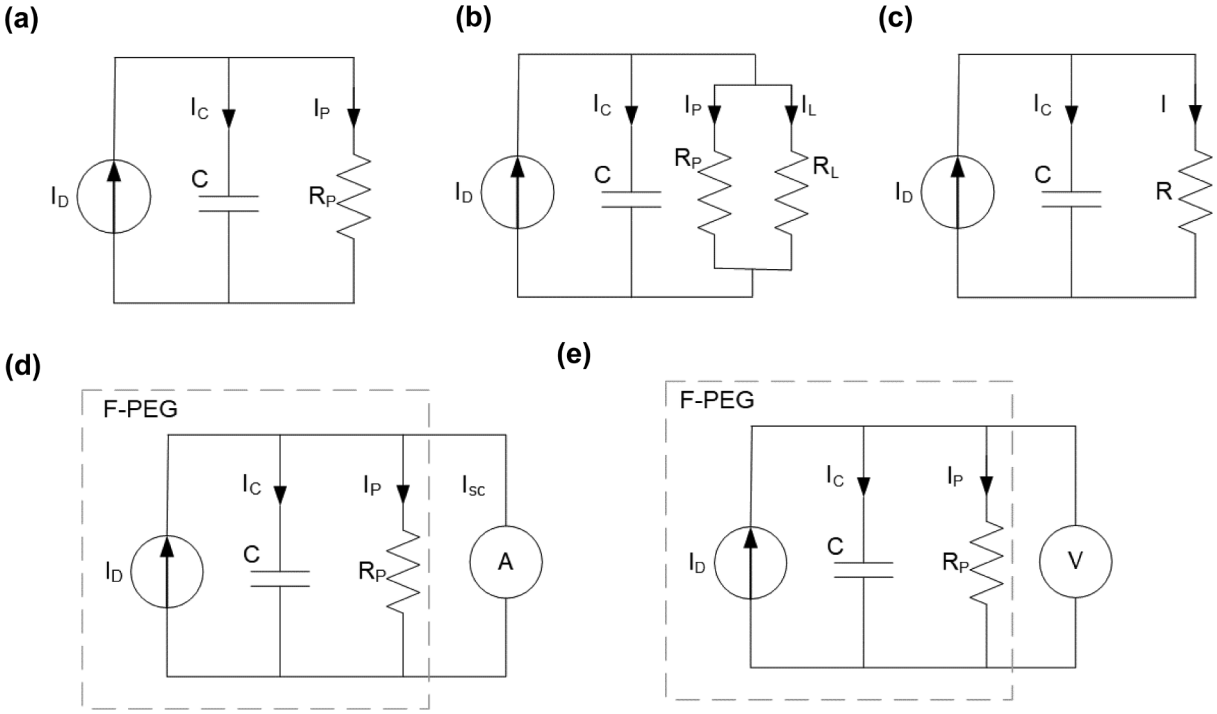

Fig. 2. Equivalent circuit of piezoelectric device (a) without load, (b) with load R_L, (c) combining the parasitic resistance R_P and load resistance R_L into a reduced resistance R, (d) current measurement, and (e) voltage measurement.

The mechanical energy W_m needed to apply strain on the piezoelectric material can be calculated [37],

$$W_m = \frac{1}{2}(At_{pz})E\varepsilon^2 \tag{8}$$

where E is the elastic modulus. The mechanical to electrical energy conversion efficiency η can be calculated,

$$\eta = \frac{W_e}{W_m} = \frac{\bar{e}^2}{\bar{k}E} \tag{9}$$

which is similar to the piezoelectric coupling coefficient of bulk piezoelectric material that quantifies the ability to convert one form of energy into another [38]. In terms of energy conversion efficiency, a high piezoelectric coefficient and low dielectric permittivity is preferred. Although the well-known PZT ferroelectric materials exhibit relatively high piezoelectric coefficients after proper electrical poling, their energy conversion efficiency is traded off with the corresponding high dielectric permittivities.

In practical applications, there will be an external load R_L on the piezoelectric device, as shown in Fig. 2b. To simplify the analysis, we can combine the parasitic resistance R_P with the load resistance R_L and use a reduced resistance R (Fig. 2c) that can be represented as,

$$R = \frac{1}{\frac{1}{R_P} + \frac{1}{R_L}} = \frac{R_P R_L}{R_P + R_L} \tag{10}$$

By analyzing the equivalent circuit, with detailed derivation shown in Supplementary Material, the piezoelectric voltage response can be written as,

$$V = V_0 e^{-Bt}\left[\int_0^t e^{Bt}\frac{d\varepsilon}{dt}dt + V_i\right] \tag{11}$$

where $V_0 = \frac{t_{pz}\bar{e}}{\bar{k}}$, with a unit of [V], $B = \frac{t_{pz}}{AR\bar{k}}$, with a unit of [1/s], and V_i is the initial condition. When B approaches zero, i.e., time constant $\tau = 1/B$ approaches infinity, the voltage response is simplified to the ideal open-circuit voltage in Eq. (6).

The corresponding piezoelectric current density J is,

$$J = \frac{V}{AR} \tag{12}$$

and the corresponding piezoelectric power density P is,

$$P = \frac{V^2}{AR} \tag{13}$$

The power consumed by the external load resistance P_L is,

$$P_L = \frac{R_P}{R_P + R_L}P \tag{14}$$

In order to increase the usable piezoelectricity, i.e., increase the power consumed by the external load resistance, the parasitic resistance should be much higher than the load resistance, $R_P \gg R_L$, so that the power consumed by the external load approaches the total piezoelectric output power. The well-known piezoelectric material zinc oxide (ZnO) was widely researched due to its biocompatibility and easy synthesis. However, the piezoelectric output of ZnO is low due to the low parasitic resistance as a result of the uncontrolled doping in ZnO, although researchers have tried to compensate or reduce the doping. PZTs also show low parasitic resistance with high leakage current within a voltage range of −10 to 10 V [39]. For III-N materials, including AlN, GaN, InN, and their alloys, the parasitic resistance can be increased by reducing the free carriers with controlled deposition process.

2.3. Buckle-bending model

Uniaxial strain in the piezoelectric thin film is of critical importance to obtain a piezoelectric response. Since most flexible piezoelectric generators works by bending mode, stress/strain in the piezoelectric thin film is modeled by mechanical bending in this study. While pure bending is preferred to create uniform strain in the piezoelectric thin film, it is difficult to apply pure bending in practice. In real tests, fixed-ended buckle-bending is widely used to bend the flexible device [23,30,40], with one end fixed and another end moved by an actuator, as shown in Fig. 3a. The strain at the buckling device center, point O in Fig. 3a, has a maximum value and can be calculated by [41],

$$\varepsilon_m = 4\pi\overline{EI}_{ratio}\frac{h}{L}\sqrt{\Delta L/L} \tag{15}$$

where

$$\overline{EI}_{ratio} = \frac{\overline{EI}_{sub}}{\overline{EI}_{ml}}$$

with $\overline{EI}_{sub}$ and $\overline{EI}_{ml}$ representing the plane-strain bending stiffness of the flexible substrate and the piezoelectric device, respectively. By attaching the piezoelectric device onto a flexible supporter with tape, as schematically shown in Supplementary Material Fig. A.2, the flexible piezoelectric device can be bent along with the supporter. For a reasonably thick supporter, the supporter can be bent almost without resistance and the $\overline{EI}_{ratio}$ can be regarded as 1. The h represents the distance of piezoelectric thin-film center to the mechanical neutral plane, as schematically illustrated in Supplementary Material, Fig. A.3a. A detailed calculation of h can be found in reference [22], with parameters shown in Supplementary Material Tables A.1 and A.2. L represents the original length of the supporter, and ΔL represents the corresponding compression with time in one buckle-bending period, as shown in Fig. 3b, which can be expressed as [40],

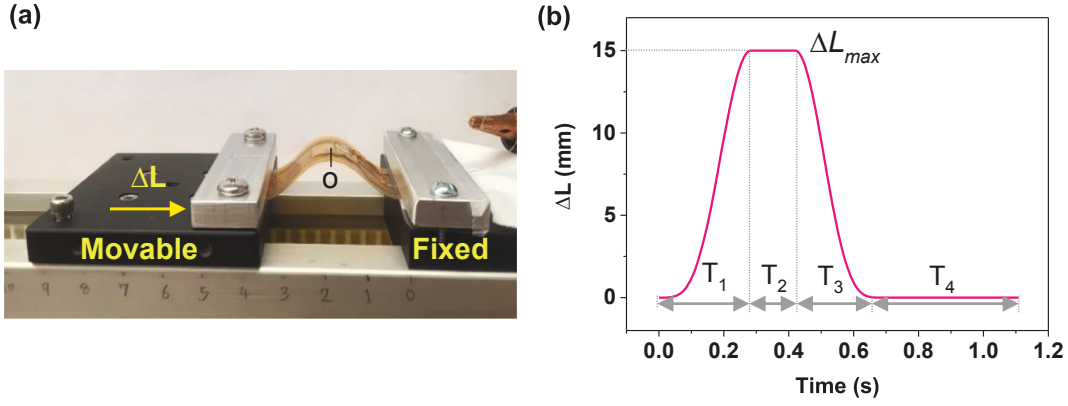

Fig. 3. Buckle-bending test. (a) Experimental setup of flexible piezoelectric device fixed-ended buckle-bending test, and (b) corresponding compression with time in a typical buckle-bending period.

$$\Delta L = \frac{\Delta L_{max}}{4}\begin{cases}\left[1-\cos\left(\frac{\pi t}{T_1}\right)\right]^2, & t\in[0,\ T_1)\\ 4, & t\in[T_1,\ T_1+T_2)\\ \left\{1-\cos\left[\frac{\pi(t-T_1-T_2-T_3)}{T_3}\right]\right\}^2, & t\in[T_1+T_2,\ T_1+T_2+T_3)\\ 0, & t\in[T_1+T_2+T_3,\ T_1+T_2+T_3+T_4)\end{cases} \tag{16}$$

In this buckle-bending model, the maximum compression ΔL_{max} characterizes the amount of bending; the compression times T_1 and T_3 characterize the speed of bending; and the holding times T_2 and T_4 characterize the idle status between bending and releasing. For symmetric buckle-bending, $T_3 = T_1$. If $T_4 = T_2 = 0$, a smaller T_1 value will correspond to a higher bending frequency at a fixed maximum compression. A large variety of mechanical bending conditions can be simulated by tuning the time constants and maximum compression. For example, the biomechanical energy like walking can be approximated with this buckle-bending model [42].

The uniaxial strain during buckle-bending varies along the horizontal direction from thin film center (point O) to thin film edge (Fig. 3a). Since the piezoelectric output depends only on the overall change of polarization in the whole thin film, an averaged strain can be used to calculate the piezoelectric output. The averaged uniaxial strain ε in the whole piezoelectric thin film can be estimated by introducing a coefficient α ($0 < \alpha < 1$),

$$\varepsilon = \alpha\varepsilon_m = \alpha 4\pi\overline{EI}_{ratio}\frac{h}{L}\sqrt{\Delta L/L} \tag{17}$$

which can be further calculated as,

$$\varepsilon = \alpha\overline{EI}_{ratio}Const\frac{1}{\pi}\begin{cases}\left[1-\cos\left(\frac{\pi t}{T_1}\right)\right], & t\in[0,\ T_1)\\ 2, & t\in[T_1,\ T_1+T_2)\\ 1-\cos\left[\frac{\pi(t-T_1-T_2-T_3)}{T_3}\right], & t\in[T_1+T_2,\ T_1+T_2+T_3)\\ 0, & t\in[T_1+T_2+T_3,\ T_1+T_2+T_3+T_4)\end{cases} \tag{18}$$

where

$$Const = 2\pi^2\frac{h}{L^{3/2}}(\Delta L_{max})^{1/2}$$

The strain rate can be calculated accordingly,

$$\frac{d\varepsilon}{dt} = \alpha\overline{EI}_{ratio}Const\begin{cases}\frac{1}{T_1}sin\left(\frac{\pi t}{T_1}\right), & t\in[0,\ T_1)\\ 0, & t\in[T_1,\ T_1+T_2)\\ \frac{1}{T_3}sin\left[\frac{\pi(t-T_1-T_2-T_3)}{T_3}\right], & t\in[T_1+T_2,\ T_1+T_2+T_3)\\ 0, & t\in[T_1+T_2+T_3,\ T_1+T_2+T_3+T_4)\end{cases} \tag{19}$$

The maximum piezoelectric surface charge density generated per bending is,

$$Q_{pz} = \bar{e}max(\varepsilon) = 4\pi\alpha\bar{e}\overline{EI}_{ratio}\frac{h}{L^{3/2}}\sqrt{\Delta L_{max}} \tag{20}$$

The ideal peak open-circuit voltage during buckle-bending is,

$$V_{ocpk} = \frac{\bar{e}}{\bar{k}}t_{pz}max(\varepsilon) = \frac{\bar{e}}{\bar{k}}t_{pz}\alpha\overline{EI}_{ratio}Const\frac{2}{\pi} = 4\pi\alpha\frac{\bar{e}}{\bar{k}}t_{pz}\overline{EI}_{ratio}\frac{h}{L^{3/2}}\sqrt{\Delta L_{max}} \tag{21}$$

The ideal peak short-circuit current density during buckle-bending is,

$$J_{scpk} = \bar{e}max\left(\frac{d\varepsilon}{dt}\right) = \bar{e}\alpha\overline{EI}_{ratio}Const\frac{1}{T_1} = 2\pi^2\alpha\bar{e}\overline{EI}_{ratio}\frac{h}{L^{3/2}}\frac{1}{T_1}\sqrt{\Delta L_{max}} \tag{22}$$

Plugging Eq. (19) into Eq. (11), the voltage response at a certain load resistance is,

$$V = \alpha\overline{EI}_{ratio}ConstV_0\begin{cases}f_1(t), & t\in[0,\ T_1)\\ f_2(t), & t\in[T_1,\ T_1+T_2)\\ f_3(t), & t\in[T_1+T_2,\ T_1+T_2+T_3)\\ f_4(t), & t\in[T_1+T_2+T_3,\ T_1+T_2+T_3+T_4)\end{cases} \tag{23}$$

where

$$f_1(t) = \frac{1}{(BT_1)^2+\pi^2}\left[BT_1sin\left(\frac{\pi t}{T_1}\right)-\pi cos\left(\frac{\pi t}{T_1}\right)\right] + \left[\frac{\pi}{(BT_1)^2+\pi^2}+V_i\right]e^{-Bt}$$

$$f_2(t) = \left[\frac{\pi}{(BT_1)^2+\pi^2}(1+e^{BT_1})+V_i\right]e^{-Bt}$$

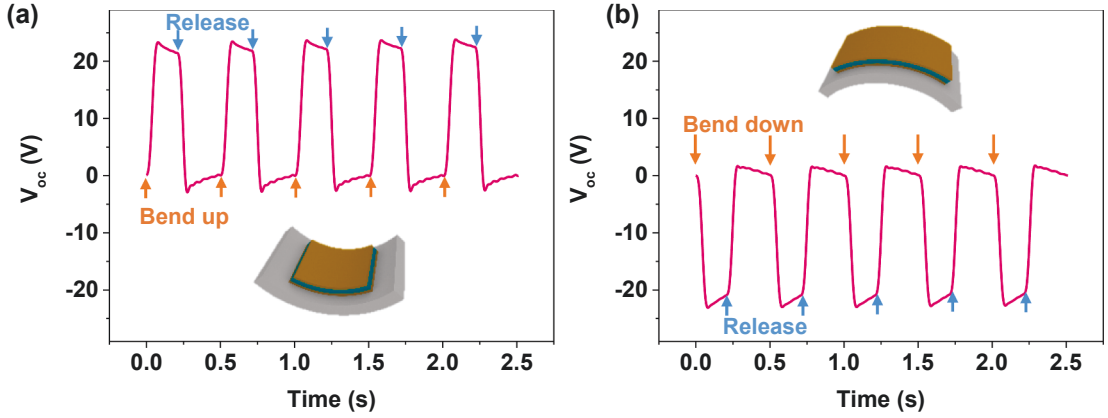

Fig. 4. Verification of piezoelectric response. Dynamic open-circuit voltage response during (a) bend up and release process and (b) bend down and release process. The inset figures in (a) and (b) illustrate the bend up and bend down conditions of the flexible piezoelectric device.

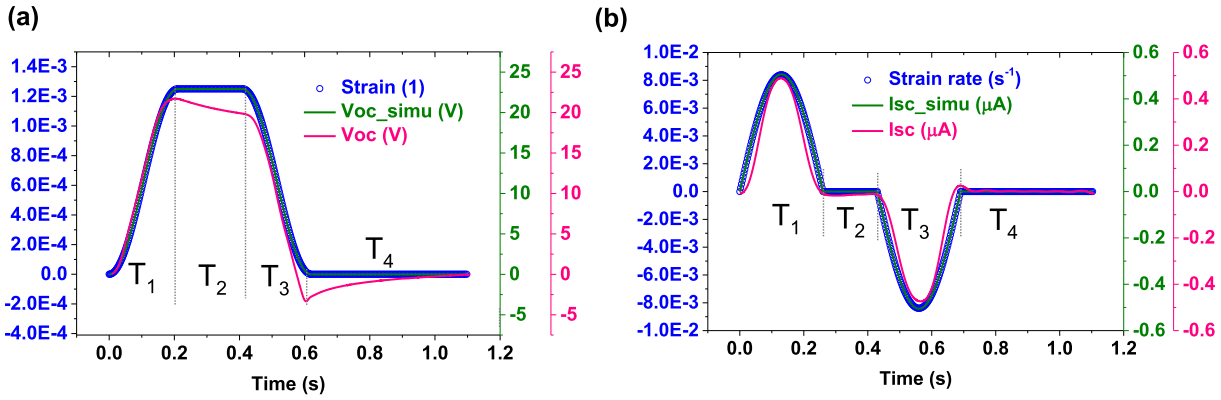

Fig. 5. Dynamic piezoelectric response during buckle-bending. (a) Simulated strain, simulated open-circuit voltage, and experimental (pink) open-circuit voltage. (b) Simulated strain rate, simulated short-circuit current, and experimental (pink) short-circuit current.

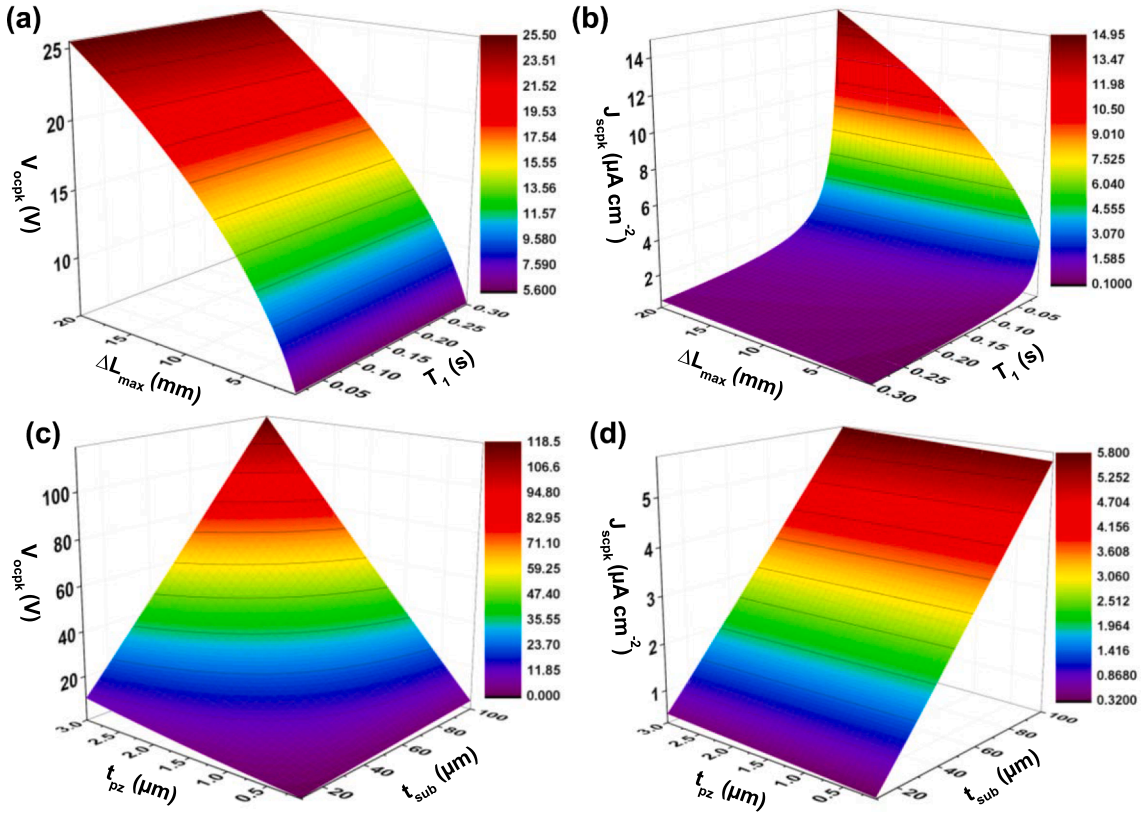

Fig. 6. Effect of mechanical bending conditions and device parameters on open-circuit voltage and short-circuit current density by numerical simulation. (a) Peak open-circuit voltage V_{ocpk} and (b) peak short-circuit current density J_{scpk} with maximum compression ΔL_{max} and compression time T_1, with a piezoelectric thin film thickness t_{pz} of 2.5 μm, and flexible substrate thickness t_{sub} of 28 μm. (c) Peak open-circuit voltage and (d) peak short-circuit current density with piezoelectric thin film and flexible substrate thickness at a maximum compression of 20 mm and compression time of 0.1 s.

$$f_3(t) = \frac{1}{(BT_3)^2+\pi^2}\left\{BT_3 sin\left[\frac{\pi(t-T_1-T_2-T_3)}{T_3}\right] - \pi cos\left[\frac{\pi(t-T_1-T_2-T_3)}{T_3}\right]\right\} + \left[\frac{\pi}{(BT_1)^2+\pi^2}(1+e^{BT_1}) - \frac{\pi}{(BT_3)^2+\pi^2}e^{B(T_1+T_2)} + V_i\right]e^{-Bt},$$

$$f_4(t) = \left[\frac{\pi}{(BT_1)^2+\pi^2}(1+e^{BT_1}) - \frac{\pi}{(BT_3)^2+\pi^2}e^{B(T_1+T_2)} - \frac{\pi}{(BT_3)^2+\pi^2}e^{B(T_1+T_2+T_3)} + V_i\right]e^{-Bt}.$$

With the voltage response, other piezoelectric output such as the current density and power density can also be obtained according to Eqs. (12) and (13)

2.4. III-N thin-film F-PEG device fabrication and test

Single-crystalline III-N thin-film, which consists of a AlN buffer layer (100 nm), $Al_xGa_{1-x}N$ interlayers (600 nm) with composition grading to manage strains during growth, and a top GaN layer (1.8 μm), was grown on Si (1 1 1) substrate by metalorganic chemical vapor deposition (MOCVD), as schematically illustrated in Supplementary Material Fig. A.4a. III-N thin-film F-PEG (with a detailed device structure shown in Supplementary Material Fig. A.3a) was fabricated with a

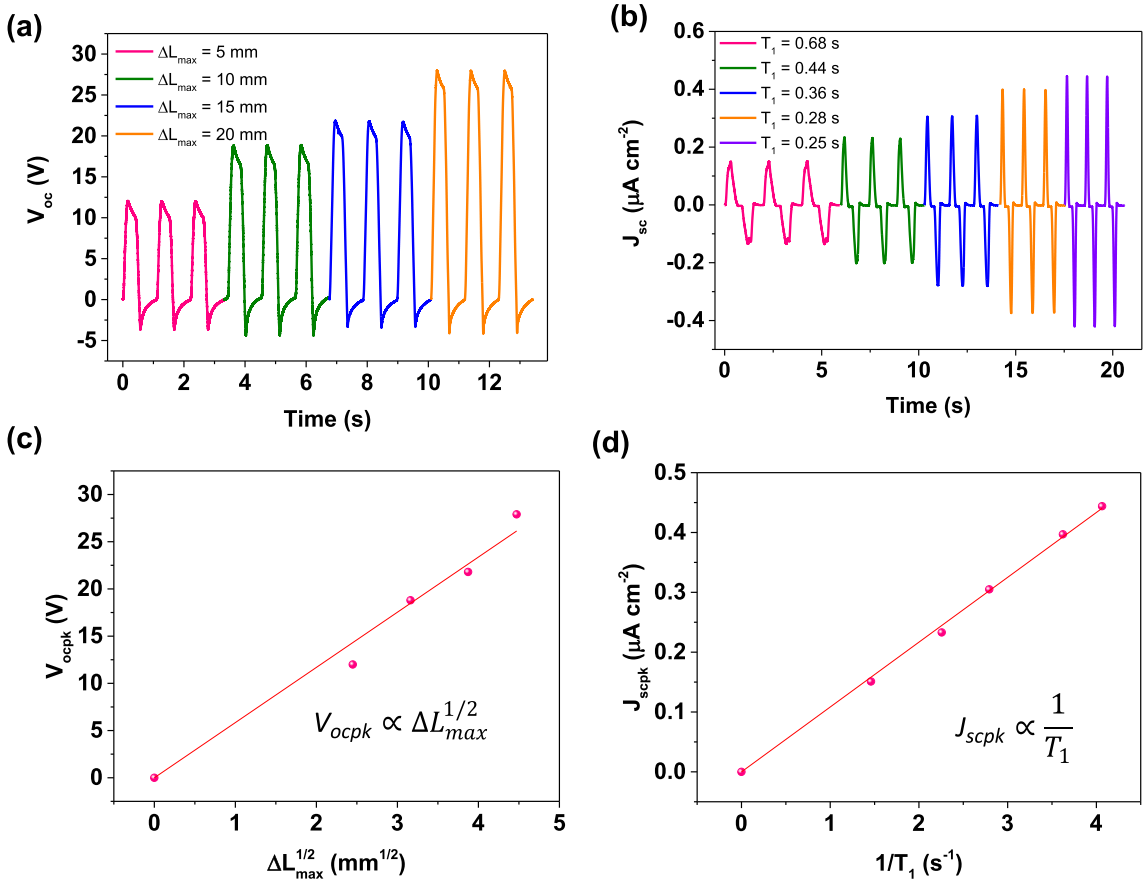

Fig. 7. Effect of mechanical bending condition on open-circuit voltage and short-circuit current density from the experiments. (a) Open-circuit voltage V_{oc} and (b) short-circuit current density J_{sc} response with time, and corresponding fitting of (c) peak open-circuit voltage V_{ocpk} with compression, and (d) peak short-circuit current density J_{scpk} with compression time.

layer-transfer method, by depositing a flexible metal substrate on III-N thin film, followed by removing the rigid Si with wet etching. Details of both III-N thin film growth conditions and F-PEG fabrication processes can be found in a previous report [22]. Copper (Cu) was used as the flexible substrate in this research due to its convenience to be deposited by electroplating.

III-N thin-film crystal structure and quality were characterized by high-resolution X-ray diffraction (HR-XRD) (D8 Discover, Bruker). The F-PEG buckle-bending test was performed on a program-controlled linear actuator (Anaheim Automation). The piezoelectric voltage and current were measured by an electrometer (Model 6514, Keithley). The current-voltage (*I-V*) characteristic curve was measured by a source meter (Model 2602B, Keithley).

3. Results and discussion

3.1. Verification of piezoelectric response

The III-N thin film used in this research has a *c*-axis crystal orientation, i.e., polarization direction perpendicular to the thin-film surface, which was verified by the XRD data shown in Supplementary Material Fig. A.4b–e. By designing a reasonably thick substrate for this research, i.e., a Cu substrate thicker than 4 μm for a 2.5 μm III-N thin film, the neutral plane is shifted out of the piezoelectric thin film (Supplementary Material Fig. A.5). This design shift results in pure negative and positive uniaxial strain in the piezoelectric thin film while being bent up and bent down (Supplementary Material Fig. A.3b). The opposite sign of strain can cause opposite change of polarization (Fig. 1b–c), i.e., opposite piezoelectric response, according to Eqs. (5) and (6). This can be confirmed experimentally by measuring the open-circuit voltage of a III-N thin-film F-PEG, as shown in Fig. 4. This test verifies the piezoelectric response and confirms the growth direction of III-N thin films, which was also brifely mentioned in our previous research [21].

3.2. Dynamic piezoelectric response

In order to test the piezoelectric performance, the electrical output was measured while buckle-bending the flexible device, as described by Fig. 3. The open-circuit voltage (V_{oc}) and short-circuit current (I_{sc}) are the basic parameters that characterize the quality of piezoelectric devices. For the as-fabricated flexible device, with an effect area of ~1 cm^2, open-circuit voltage and short-circuit current were simulated and measured with a designated buckle-bending process.

The III-N thin film uniaxial strain and strain rate and the piezoelectric device open-circuit voltage and short-circuit current were simulated according to Eq. (18), Eq. (19), Eq. (6), and Eq. (5), respectively, which are shown in Fig. 5. The simulated open-circuit voltage response follows the trend of strain response (Fig. 5a) since they are related by a coefficient. Similarly, the simulated short-circuit current response follows the strain rate (Fig. 5b).

The experimental open-circuit voltage roughly follows the simulated one, except when showing a voltage decay during the two strain-holding periods (i.e., T_2 and T_4 sub-periods), as shown in Fig. 5a. The voltage decay is a result of piezoelectric charge leakage through the internal resistance of the device and external measurement circuit, both of which are not infinitely high. A current on the scale of nA can leak through the III-N thin film piezoelectric device in the voltage range of −40 V to 40 V, as indicated by the *I-V* characteristics in Supplementary Material Fig. A.6. The impedance of the Keithley 6514 electrometer

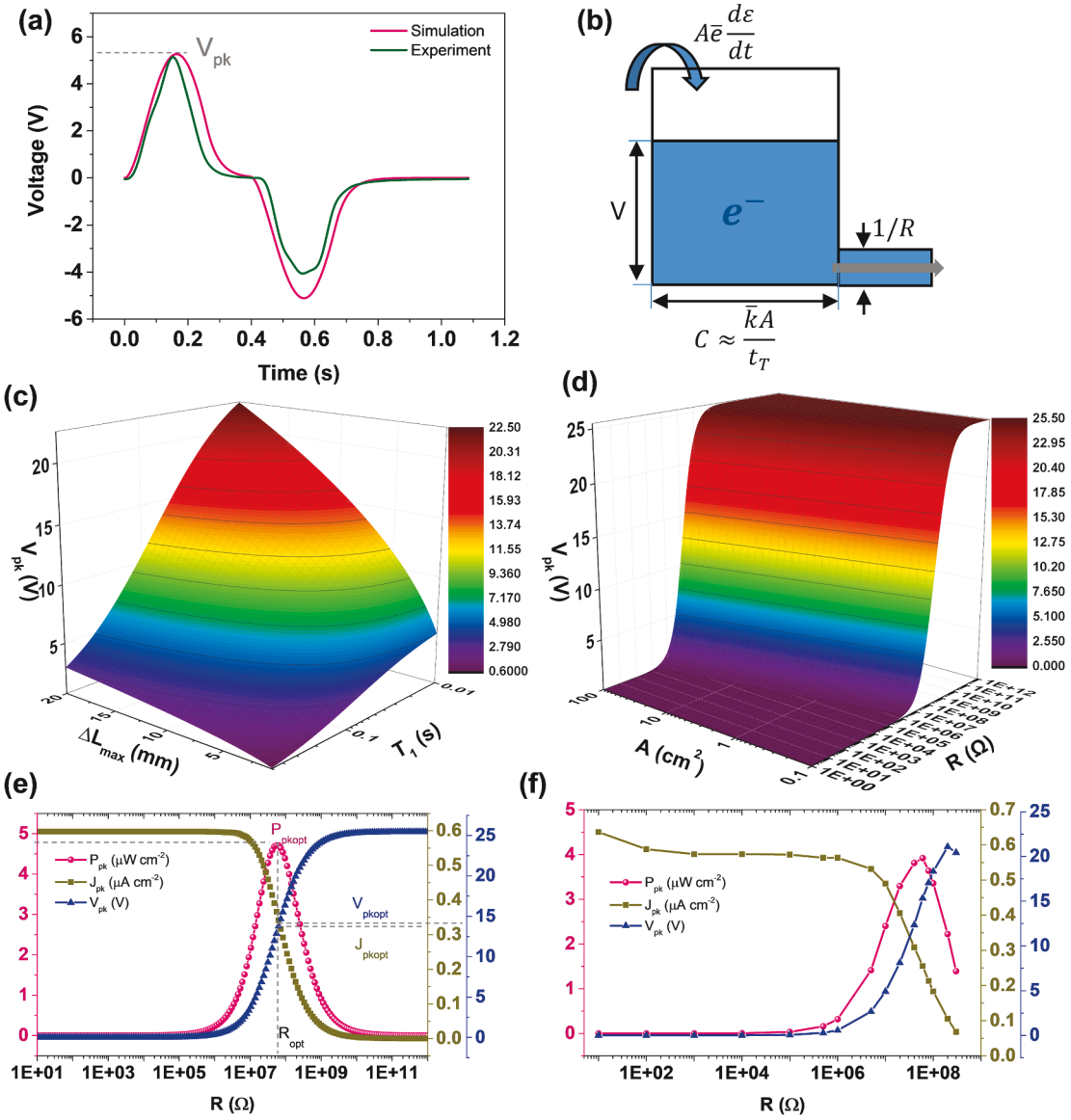

Fig. 8. Piezoelectric response with a load resistance. (a) Voltage response at a load resistance of 10 MΩ. (b) Schematic illustration of the piezoelectric voltage depends on piezoelectric charge accumulation. Simulated peak voltage V_{pk} with (c) maximum compression ΔL_{max} and compression time T_1, and with (d) device area A and load resistance R. (e) Simulated and (f) experimental peak voltage V_{pk}, peak current density J_{pk}, and peak power density P_{pk} with load resistance, showing a maximum peak power density P_{pkopt}, at an optimum load resistance R_{opt}, with a corresponding optimum peak voltage V_{pkopt}, and optimum peak current density J_{pkopt}. $T_1 = 0.25$ s, $\Delta L_{max} = 20$ mm, $t_{sub} = 28$ μm.

used to measure the open-circuit voltage is 200 TΩ, corresponding to a current leakage less than 1 pA within the voltage range of 200 V. Thus, the minimal voltage decay is mainly caused by the electric charge leakage through the piezoelectric device.

The experimentally measured short-circuit response well matches the simulated one (Fig. 5b) since the external circuit is shorted, through which most of the piezoelectric charge will go and be measured. Since the applied compression on the flexible device by the linear actuator during buckle-bending is not exactly the same as the function input due to inertia and friction, the experimental short-circuit response shape is slightly different from the simulation.

3.3. Effect of mechanical bending and device parameters on open-circuit voltage and short-circuit current density

The open-circuit voltage and short-circuit density are the basic output parameters that characterize piezoelectric device performance. These parameters can be tuned by both external mechanical bending and the internal device parameters. For a designated piezoelectric device with fixed device parameters, such as the thickness of the piezoelectric thin film and flexible substrate, the piezoelectric output can be tuned by mechanical bending, which is related to the source of mechanical energy to be harvested. The ideal peak open-circuit voltage V_{ocpk} – and similarly the maximum strain – increases with the square root of maximum compression ΔL_{max} and is independent of the time it takes to reach the maximum strain, as described by Eq. (21) and shown in Fig. 6a. The ideal peak short-circuit current density J_{scpk} not only increases with the square root of maximum compression, but also increases with the inverse of the compression time $1/T_1$, as described by Eq. (22) and shown in Fig. 6b.

For a certain type of mechanical energy condition in practical applications, the degree of bending and bending speed applied on the flexible piezoelectric device are roughly fixed, and can be approximated by a fixed ΔL_{max} and T_1 in this simulation. Under this designated mechanical energy condition, the piezoelectric output can still be tuned by designing the device parameters such as the thickness of the

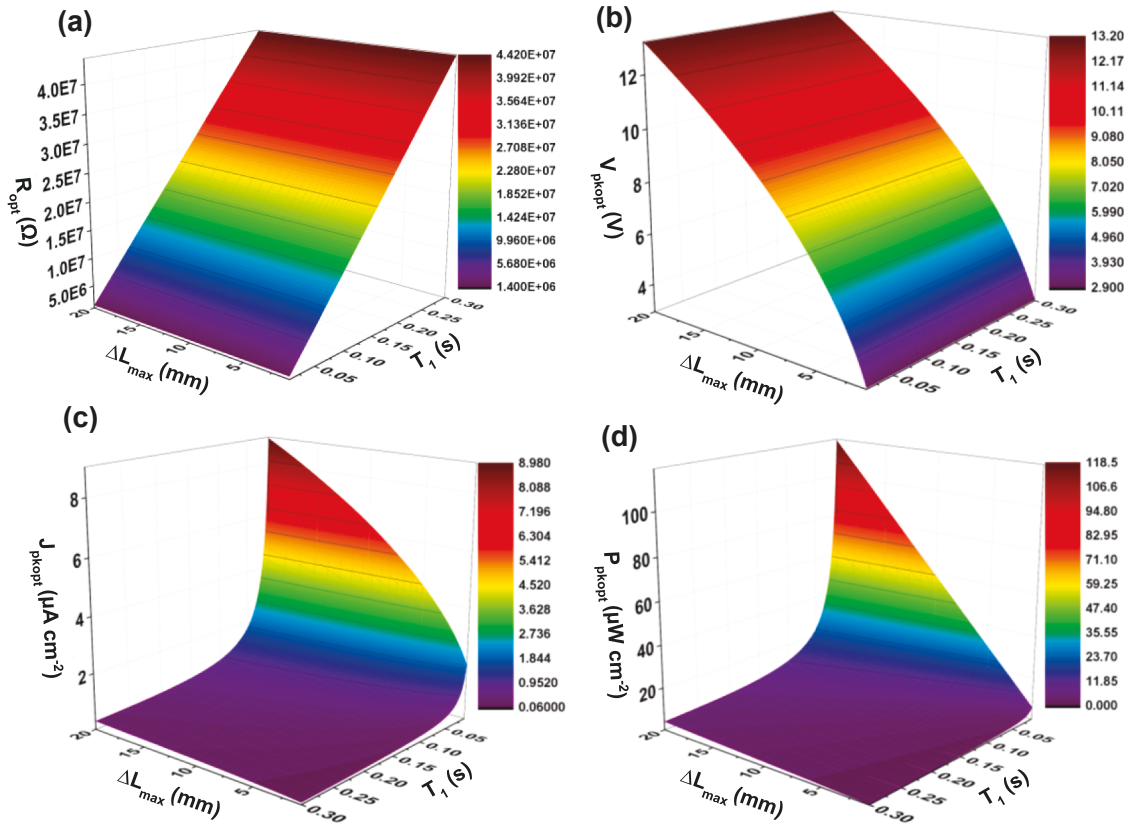

Fig. 9. Effect of mechanical bending on optimum piezoelectric output. (a) Optimum load resistance R_{opt}, and corresponding (b) optimum peak voltage V_{pkopt}, (c) optimum peak current density J_{pkopt}, and (d) optimum peak power density P_{pkopt} with maximum compression ΔL_{max} and compression time T_1.

piezoelectric thin film and flexible substrate. With the neutral plane lying outside of the piezoelectric thin film, the peak open-circuit voltage increases linearly with both the thickness of the piezoelectric thin film and the thickness of the flexible substrate (Fig. 6c), as does the maximum thin film strain. The peak short-circuit current density increases linearly mainly with the flexible substrate thickness and slightly with the piezoelectric thin film thickness, as shown in Fig. 6d.

The experimental open-circuit voltage (Fig. 7a) and short-circuit current density (Fig. 7b) were measured at different bending conditions in order to verify the validity of the numerical simulation. The experimental results of the open-circuit voltage and short-circuit current density are comparable to the simulation, with the peak open-circuit voltage proportional to the square root of maximum compression (Fig. 7c), and the peak short-circuit current density proportional to the inverse of the compression time (Fig. 7d).

3.4. Effect of load resistance on piezoelectric output

For generator applications, an external load resistance will be connected to the piezoelectric device. Even without applying an intentional external load during the piezoelectric device measurement, a low internal impedance of the electrometer can be seen as a load resistance. Under these circumstances, the piezoelectric output deviates from the ideal open-circuit and short-circuit condition and are described by Eqs. (11)–(13). A typical piezoelectric voltage response with a limited load resistance is shown in Fig. 8a, showing a peak voltage in each bending period. The voltage is determined by the accumulation of piezoelectric charge, as schematically illustrated in Fig. 8b. On the one hand, the piezoelectric charge, i.e., the driving source of piezoelectricity, is pumped into the device and the pumping speed is proportional to the device area and strain rate. On the other hand, the piezoelectric charge continuously leaks through the load resistance. The voltage of the piezoelectric device with a load resistance is determined by the overall build-up of the electric charge. By increasing the bending speed, which can be accomplished by increasing maximum compression and decreasing compression time, the peak voltage increases until approaches the ideal open-circuit voltage limit, as shown in Fig. 8c. Also, by increasing the device area, the peak voltage will increase until approach the ideal open-circuit voltage limit (Fig. 8d).

Unlike the voltage that monotonically increases with load resistance and the current that monotonically decreases with load resistance, the power, which is the product of the current and voltage, shows a maximum point at a certain load resistance, e.g., the optimum load resistance or matching resistance as shown in Fig. 8e, with a corresponding optimum peak power density, optimum peak voltage, and optimum peak current density. The variation of piezoelectric output with load resistance was confirmed by the experimental results shown in Fig. 8f. In practical piezoelectric generator designs, especially for the system level applications, the device optimum load resistance should be designed to match the load resistance such that the piezoelectric output power can be maximized. The optimum piezoelectric output can be tuned by both the external mechanical bending conditions and the device parameters.

3.5. Effect of mechanical bending conditions on optimum piezoelectric output

For a designated flexible piezoelectric device with a fixed piezoelectric thin film thickness, flexible substrate thickness, and device area, the optimum piezoelectric output can be controlled by the mechanical bending conditions. The optimum load resistance increases linearly with compression time, however, it does not change with maximum compression, as shown in Fig. 9a. Similar to the ideal peak open-circuit voltage (Fig. 6a), the optimum peak voltage is also

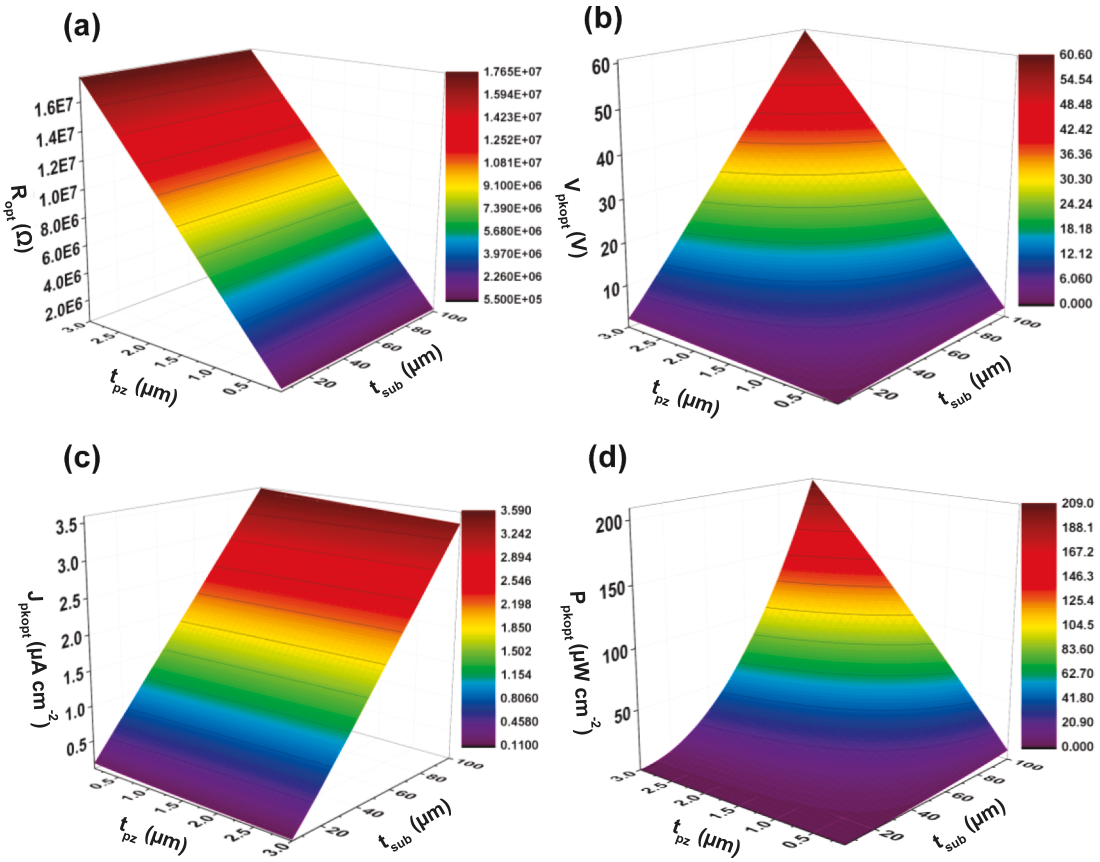

Fig. 10. Effect of device thickness on optimum piezoelectric output. (a) Optimum load resistance R_{opt}, and corresponding (b) optimum peak voltage V_{pkopt}, (c) optimum peak current density J_{pkopt}, and (d) optimum peak power density P_{pkopt} with piezoelectric thin film thickness t_{pz} and flexible substrate thickness t_{sub}.

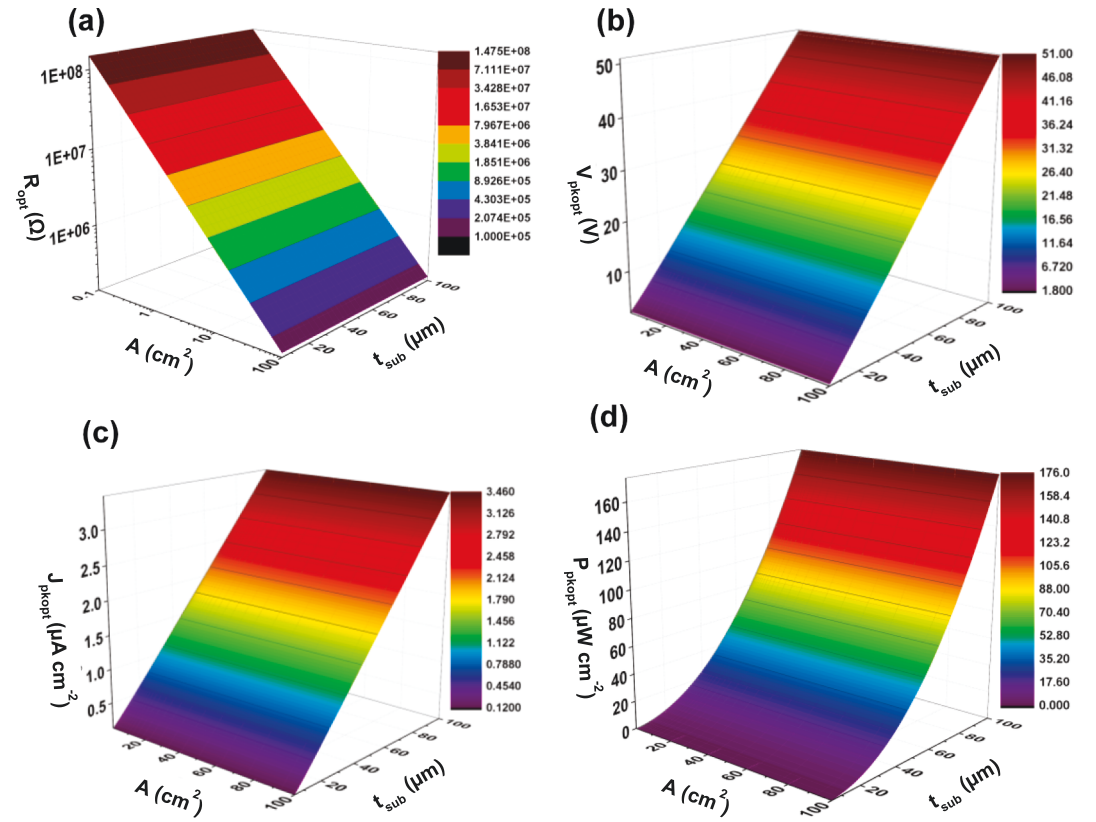

Fig. 11. Effect of device size on optimum piezoelectric output. (a) Optimum load resistance R_{opt}, and corresponding (b) optimum peak voltage V_{pkopt}, (c) optimum peak current density J_{pkopt}, and (d) optimum peak power density P_{pkopt} with device area A and flexible substrate thickness t_{sub}.

proportional to square root of the maximum compression and it does not change with compression time (Fig. 9b). The optimum peak current density is also proportional to the square root of maximum compression and inverse of the compression time (Fig. 9c), like the ideal peak short-circuit current (Fig. 6b). Combining the change of voltage and current, the optimum peak power density increases linearly with the maximum compression and the inverse of the compression time (Fig. 9d).

3.6. Effect of device parameters on optimum piezoelectric output

For a designated mechanical energy source, the available amount of bending and bending speed to the flexible piezoelectric device is almost fixed. The optimum piezoelectric output can be tuned by designing the device parameters. The optimum load resistance increases linearly with the piezoelectric thin film thickness, and it does not change with flexible substrate thickness (Fig. 10a). Like the effect on ideal peak open-circuit voltage (Fig. 6c), the optimum peak voltage increases linearly with both the piezoelectric thin film thickness and the flexible substrate thickness (Fig. 10b). Also, like the change of ideal peak short-circuit current density (Fig. 6d), the optimum peak current density is mainly proportional to the flexible substrate thickness (Fig. 10c). However, the optimum peak current density slightly decreases with the piezoelectric thin film thickness, which is just the opposite of the ideal short-circuit current density. Combining the effects of voltage and current, the optimum peak power density increases with the square of flexible substrate thickness and linearly with piezoelectric thin film thickness, as shown in Fig. 10d. In practical applications, if two load devices are connected in series, the load resistance, required voltage and power will be twice as much, while the current will be the same. A F-PEG with a twice piezoelectric materials thickness can be designed for this application.

The optimum piezoelectric output can also be tuned by the effective device area, i.e., the area on which piezoelectric charge can be collected. Increasing the device area decreases the optimum load resistance with a inverse relationship (Fig. 11a), however, it does not change the corresponding optimum peak voltage (Fig. 11b), optimum peak current density (Fig. 11c), and optimum peak power density (Fig. 11d). In other words, at the same mechanical bending condition, the optimum current and optimum power can be scaled with device area without changing the optimum voltage. In practical applications, if two load devices are connected in parallel, the load resistance will be half, the required voltage will not change, while the required current and power will be twice. A F-PEG with a twice device area can be designed for this application.

4. Conclusions

A clear understanding of the output behaviors of flexible piezoelectric generators is helpful to optimize the device design and related systems for specific applications. Output characteristics of flexible piezoelectric generators were systematically investigated numerically with a buckle-bending model, and they were verified experimentally using group III-nitride thin-film piezoelectric generators. For a designated device, the piezoelectric output can be tuned with a detailed relationship by external mechanical bending conditions, such as bending extent and bending speed. At a specific mechanical energy condition, the piezoelectric output can be tuned with a detailed relationship by the device parameters, such as the piezoelectric thin film and substrate thickness, as well as the device area. Since the piezoelectric output depends on a combination of device parameters and mechanical conditions, detailed device structure and test conditions should be provided in order to evaluate the device performance. The optimum load resistance of piezoelectric generators is typically higher than conventional electromagnetic generators due to limited displacement currents. A higher optimum load resistance can keep the voltage higher and make full use of the piezoelectric charges. The optimum load resistance can be tuned to a target value with a detailed relationship by changing the device area and bending speed. Since the optimum voltage, current density, and power density do not change with device area, the overall output current and power can be scaled linearly with device area, as long as the device works with an optimum load resistance. Although the data was obtained using III-N thin-film, the output characteristics are still helpful for designing flexible piezoelectric generators using other types of materials since the working mechanism is the same.

Acknowledgements

This work is partially supported by King Abdullah University of Science and Technology (KAUST), Saudi Arabia (Contract No. OSR-2017-CRG6-3437.02) and National Science Foundation, United States of America (Grant No. 1842299). J.H.R. also acknowledges partial support from the Texas Center for Superconductivity at the University of Houston (TcSUH), USA.

Appendix A. Supplementary material

Supplementary data to this article can be found online at https://doi.org/10.1016/j.apenergy.2019.113856.

References

[1] Khan Y, Ostfeld AE, Lochner CM, Pierre A, Arias AC. Monitoring of vital signs with flexible and wearable medical devices. Adv Mater 2016;28:4373–95. https://doi.org/10.1002/adma.201504366.
[2] Zhang R, Lin L, Jing Q, Wu W, Zhang Y, Jiao Z, et al. Nanogenerator as an active sensor for vortex capture and ambient wind-velocity detection. Energy Environ Sci 2012;5:8528–33. https://doi.org/10.1039/C2EE22354F.
[3] Wang ZL. Towards self-powered nanosystems: from nanogenerators to nanopiezotronics. Adv Funct Mater 2008;18:3553–67. https://doi.org/10.1002/adfm.200800541.
[4] Lee M, Bae J, Lee J, Lee C-S, Hong S, Wang ZL. Self-powered environmental sensor system driven by nanogenerators. Energy Environ Sci 2011;4:3359–63. https://doi.org/10.1039/C1EE01558C.
[5] Fan F-R, Tian Z-Q, Lin Wang Z. Flexible triboelectric generator. Nano Energy 2012;1:328–34. https://doi.org/10.1016/j.nanoen.2012.01.004.
[6] Wang ZL. Triboelectric nanogenerators as new energy technology for self-powered systems and as active mechanical and chemical sensors. ACS Nano 2013;7:9533–57. https://doi.org/10.1021/nn404614z.
[7] Wang X. Piezoelectric nanogenerators-Harvesting ambient mechanical energy at the nanometer scale. Nano Energy 2012;1:13–24. https://doi.org/10.1016/j.nanoen.2011.09.001.
[8] Wang ZL, Song J. Piezoelectric nanogenerators based on zinc oxide nanowire arrays. Science 2006;312:242–6. https://doi.org/10.1126/science.1124005.
[9] Starner T. Human-powered wearable computing. IBM Syst J 1996;35:618–29. https://doi.org/10.1147/sj.353.0618.
[10] Donelan JM, Li Q, Naing V, Hoffer JA, Weber DJ, Kuo AD. Biomechanical energy harvesting: generating electricity during walking with minimal user effort. Science 2008;319:807–10. https://doi.org/10.1126/science.1149860.
[11] Park K-I, Son JH, Hwang G-T, Jeong CK, Ryu J, Koo M, et al. Highly-efficient, flexible piezoelectric PZT thin film nanogenerator on plastic substrates. Adv Mater 2014;26:2514–20. https://doi.org/10.1002/adma.201305659.
[12] Hwang GT, Park H, Lee JH, Oh S, Park KI, Byun M, et al. Self-powered cardiac pacemaker enabled by flexible single crystalline PMN-PT piezoelectric energy harvester. Adv Mater 2014;26:4880–7. https://doi.org/10.1002/adma.201400562.
[13] Lu X, Qu H, Skorobogatiy M. Piezoelectric micro-and nanostructured fibers fabricated from thermoplastic nanocomposites using a fiber drawing technique: comparative study and potential applications. ACS Nano 2017;11:2103–14. https://doi.org/10.1021/acsnano.6b08290.
[14] Wan C, Bowen CR. Multiscale-structuring of polyvinylidene fluoride for energy harvesting: the impact of molecular-, micro- and macro-structure. J Mater Chem A 2017;5:3091–128. https://doi.org/10.1039/C6TA09590A.
[15] Koka A, Zhou Z, Sodano HA. Vertically aligned BaTiO3 nanowire arrays for energy harvesting. Energy Environ Sci 2014;7:288–96. https://doi.org/10.1039/C3EE42540A.
[16] Gao T, Liao J, Wang J, Qiu Y, Yang Q, Zhang M, et al. Highly oriented BaTiO3 film self-assembled using an interfacial strategy and its application as a flexible piezoelectric generator for wind energy harvesting. J Mater Chem A 2015;3:9965–71. https://doi.org/10.1039/C5TA01079A.
[17] Wu JM, Xu C, Zhang Y, Wang ZL. Lead-free nanogenerator made from single ZnSnO3 microbelt. ACS Nano 2012;6:4335–40. https://doi.org/10.1021/nn300951d.
[18] Wu JM, Xu C, Zhang Y, Yang Y, Zhou Y, Wang ZL. Flexible and transparent nanogenerators based on a composite of lead-free ZnSnO3 triangular-belts. Adv Mater

2012;24:6094–9. https://doi.org/10.1002/adma.201202445.
[19] Hu Y, Lin L, Zhang Y, Wang ZL. Replacing a battery by a nanogenerator with 20 V output. Adv Mater 2012;24:110–4. https://doi.org/10.1002/adma.201103727.
[20] Kim D, Lee KY, Gupta MK, Majumder S, Kim SW. Self-compensated insulating ZnO-based piezoelectric nanogenerators. Adv Funct Mater 2014;24:6949–55. https://doi.org/10.1002/adfm.201401998.
[21] Chen J, Oh SK, Zou H, Shervin S, Wang W, Pouladi S, et al. High-output lead-free flexible piezoelectric generator using single-crystalline GaN thin film. ACS Appl Mater Interfaces 2018;10:12839–46. https://doi.org/10.1021/acsami.8b01281.
[22] Chen J, Oh SK, Nabulsi N, Johnson H, Wang W, Ryou J-H. Biocompatible and sustainable power supply for self-powered wearable and implantable electronics using III-nitride thin-film-based flexible piezoelectric generator. Nano Energy 2019;57:670–9. https://doi.org/10.1016/j.nanoen.2018.12.080.
[23] Johar MA, Kang J-H, Hassan MA, Ryu S-W. A scalable, flexible and transparent GaN based heterojunction piezoelectric nanogenerator for bending, air-flow and vibration energy harvesting. Appl Energy 2018;222:781–9. https://doi.org/10.1016/j.apenergy.2018.04.038.
[24] Dudem B, Kim DH, Bharat LK, Yu JS. Highly-flexible piezoelectric nanogenerators with silver nanowires and barium titanate embedded composite films for mechanical energy harvesting. Appl Energy 2018;230:865–74. https://doi.org/10.1016/j.apenergy.2018.09.009.
[25] Guo L, Lu Q. Numerical analysis of a new piezoelectric-based energy harvesting pavement system: Lessons from laboratory-based and field-based simulations. Appl Energy 2019;235:963–77. https://doi.org/10.1016/j.apenergy.2018.11.037.
[26] Liu M, Lin R, Zhou S, Yu Y, Ishida A, Mcgrath M, et al. Design, simulation and experiment of a novel high efficiency energy harvesting paver. Appl Energy 2018;212:966–75. https://doi.org/10.1016/j.apenergy.2017.12.123.
[27] Yang Z, Zu J. Comparison of PZN-PT, PMN-PT single crystals and PZT ceramic for vibration energy harvesting. Energy Convers Manage 2016;122:321–9. https://doi.org/10.1016/j.enconman.2016.05.085.
[28] Bowen CR, Kim HA, Weaver PM, Dunn S. Piezoelectric and ferroelectric materials and structures for energy harvesting applications. Energy Environ Sci 2014;7:25–44. https://doi.org/10.1039/C3EE42454E.
[29] Wu JG, Shi HD, Zhao TL, Yu Y, Dong SX. High-temperature BiScO3-PbTiO3 piezoelectric vibration energy harvester. Adv Funct Mater 2016;26:7186–94. https://doi.org/10.1002/adfm.201602645.
[30] Dagdeviren C, Yang BD, Su Y, Tran PL, Joe P, Anderson E, et al. Conformal piezoelectric energy harvesting and storage from motions of the heart, lung, and diaphragm. Proc Natl Acad Sci USA 2014;111:1927–32. https://doi.org/10.1073/pnas.1317233111.
[31] Martin RM. Piezoelectricity. Phys Rev B 1972;5:1607. https://doi.org/10.1103/PhysRevB.5.1607.
[32] Lee EJ, Kim TY, Kim S-W, Jeong S, Choi Y, Lee SY. High-performance piezoelectric nanogenerators based on chemically-reinforced composites. Energy Environ Sci 2018;11:1425–30. https://doi.org/10.1039/C8EE00014J.
[33] Wang ZL. On Maxwell's displacement current for energy and sensors: the origin of nanogenerators. Mater Today 2017;20:74–82. https://doi.org/10.1016/j.mattod.2016.12.001.
[34] Ali WG, Ibrahim SW. Power analysis for piezoelectric energy harvester. Energy Power Eng 2012;4:496. https://doi.org/10.4236/epe.2012.46063.
[35] Lee S, Bae SH, Lin L, Yang Y, Park C, Kim SW, et al. Super-flexible nanogenerator for energy harvesting from gentle wind and as an active deformation sensor. Adv Funct Mater 2013;23:2445–9. https://doi.org/10.1002/adfm.201202867.
[36] Zhang G, Zhao P, Zhang X, Han K, Zhao T, Zhang Y, et al. Flexible three-dimensional interconnected piezoelectric ceramic foam based composites for highly efficient concurrent mechanical and thermal energy harvesting. Energy Environ Sci 2018;11:2046–56. https://doi.org/10.1039/C8EE00595H.
[37] Beer FP, E. Russell Johnston J, Dewolf JT, Mazurek DF. Mechanics of materials. 6th ed. New York: McGraw-Hill; 2012.
[38] Vijaya M. Piezoelectric materials and devices: applications in engineering and medical sciences. 1st ed. Boca Raton: CRC Press; 2016.
[39] Kingon AI, Srinivasan S. Lead zirconate titanate thin films directly on copper electrodes for ferroelectric, dielectric and piezoelectric applications. Nat Mater 2005;4:233. https://doi.org/10.1038/nmat1334.
[40] Su YW, Dagdeviren C, Li R. Measured output voltages of piezoelectric devices depend on the resistance of voltmeter. Adv Funct Mater 2015;25:5320–5. https://doi.org/10.1002/adfm.201502280.
[41] Dagdeviren C, Joe P, Tuzman OL, Park K-I, Lee KJ, Shi Y, et al. Recent progress in flexible and stretchable piezoelectric devices for mechanical energy harvesting, sensing and actuation. Extreme Mech Lett 2016;9:269–81. https://doi.org/10.1016/j.eml.2016.05.015.
[42] Grimmer M, Eslamy M, Seyfarth A. Energetic and Peak Power Advantages of Series Elastic Actuators in an Actuated Prosthetic Leg for Walking and Running. Actuators 2014;3:1–19. https://doi.org/10.3390/act3010001.